Oral presentation | Incompressible/compressible/hypersonic flow
Incompressible/compressible/hypersonic flow-V
Fri. Jul 19, 2024 10:45 AM - 12:45 PM Room D

[13-D-01] Shock-fitting and shock-capturing simulations of transonic flows in a channel with a half lenticular profile

Aldo Bonfiglioli[1], *Renato Paciorri[2], Alessia Assonitis[2] （1. Università degli studi della Basilicata , 2. Università di Roma La Sapienza ）

Keywords: Shock-fitting, Transonic flow, Shock-capturing

©Retained by Authors

Twelfth International Conference on
Computational Fluid Dynamics (ICCFD12),
Kobe, Japan, July 14-19, 2024

Shock-fitting and shock-capturing simulations of transonic flows in a channel with a half lenticular profile

A. Bonfiglioli*, R. Paciorri** and A. Assonitis*,**
Corresponding author: renato.paciorri@uniroma1.it
* University of Basilicata, Italy.
** University of Rome "La Sapienza", Italy.

Abstract: The present study focuses on particular properties of transonic flows through a planar channel featuring a circular bump on the lower wall. The selected geometry is reminiscent of the region surrounding the trailing edge of an airfoil at zero angle-of-attack and the resulting flow pattern is indeed similar to the fishtail shock-pattern that characterizes airfoils flying at nearly sonic speed. Numerical simulations have been conducted by solving the inviscid Euler equations using both a commercial and an in-house CFD code; discontinuities are modeled using shock-capturing in the former and shock-fitting in the latter. Numerical experiments reveal different shock-patterns obtained by independently varying the pressure ratio defined as the ratio between the static outlet pressure and the inlet total pressure. When shock-interactions occur, shock-polar analysis reveals that the branching point can be modeled using either von Neumann's three-shock-theory or Guderley's four-wave-theory, depending on the pressure ratio. Furthermore, for certain values of the pressure ratio, double solutions have been observed.

Keywords: Shock-shock interaction, Mach interaction Shock-capturing, Shock-fitting.

1 Introduction

In previous studies [1, 2], the authors analyzed the so-called "fishtail" shock-pattern that characterizes the transonic flow past a NACA0012 airfoil at zero incidence and for M_∞ ranging between 0.91 to 0.95. Figure 1 shows a visualization of the fishtail shock-pattern in the upper half of the flow-field. It consists in two oblique shock waves that originate at the trailing edge (TE) of the airfoil and a nearly normal shock standing behind the TE; the two oblique shocks (only one is visible in Fig. 1) and the normal shock merge at two branching points (one of these is denoted with a black circle in Fig. 1) which resemble the

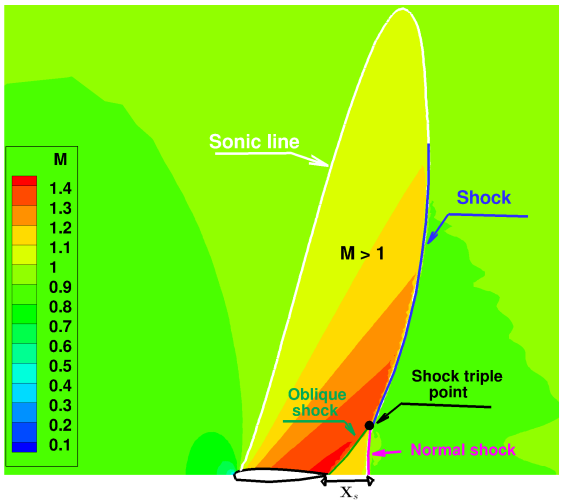

Figure 1: Transonic flow past a NACA0012 airfoil at $M_\infty = 0.95$ and fishtail shock-structure

triple-point that is observed in steady and un-steady Mach reflections. Mach reflections can be modeled

using either von Neumann's three-shock theory [3, 4] (3ST) or the four-wave theory (4WT), known in the literature as Guderley's model [5].

In the present paper, we study the transonic flow in a two-dimensional planar channel featuring a lenticular bump on the lower wall. The geometry resembles the region close to the TE of an airfoil and the shock-pattern that arises is indeed very similar to the fishtail shock-structure we have previously described. One of the advantages in simulating an internal flow, as we do in this paper, is that it allows to use a much smaller computational domain than that required to simulate the external flow past an airfoil.

Numerical computations have been performed using two different CFD codes: the commercial shock-capturing code `CFD++` [6] and the in-house, open-source, shock-fitting code `UnDiFi-2D`, which has been developed by the authors [7].

The present study is organized as follows. Sect. 2 recalls both von Neumann's 3ST and Guderley's 4WT and also introduces the (M_1, σ_{12}) plane which allows to parametrically define the domain of existence of the 3ST and 4WT. Sect. 2.3 briefly describes the gasdynamic solvers used in the simulations. Sect. 3 gives the definition of the test-cases and illustrates the properties of the computational meshes. Numerical results and flow analyses are reported in Sect. 4. Final considerations and remarks will be given in Sect. 5.

2 Generalities

2.1 Shock-interaction modelling: three-shock theory (3ST) and four-wave theory (4WT)

von Neumann's 3ST is used to analytically model the triple-point that occurs in Mach reflections (MR), see the sketch in Fig. 2a. The shock-pattern in the neighborhood of the branching points of the fishtail shock-structure of Fig. 1 can also be described by borrowing the nomenclature used for Mach reflections. This is done in Fig. 2b, where the oblique shock emerging from the trailing edge of the airfoil is the I-shock, which can be thought of as being "reflected" from the far field, thus giving rise to the nearly normal shocks (the R-shock). Beyond the branching point where the oblique and nearly normal shocks interact, the former bends into the M-shock and the dashed line represents the contact-discontinuity or slip-stream (SS).

The non-linear algebraic equations governing the 3ST can be found in either [8, § 135] or [9, § 1.3.2] and consist in the Rankine-Hugoniot jump relations for all three shocks, supplemented by the condition of parallel streams and equal pressure across the contact discontinuity. The number of unknowns matches that of the available equations once three parameters are given. We assign: *i*) the adiabatic index, γ, of the gas (here always set equal to 1.4); *ii*) the Mach number, M_1, ahead of the I-shock and *iii*) a measure of the I-shock strength, which we here choose to be the I-shock angle, σ_{12}.

Solutions to the 3ST can be graphically found by seeking intersections between the I- and R-shock polar in the pressure-deflection (θ, ξ) plane, shown in the central frame of Figure 2; for given values of γ and M_1, an unique shock polar can be drawn.

Whenever the I- and R-shock polar do not intersect, as in Fig. 3a, von Neumann's 3ST has no solution and a different analytical model must be used. In [5, 10] Guderley proposed the addition of a centred, isentropic expansion fan (EF) or Prandtl-Mayer (PM) wave that accelerates the flow from sonic conditions behind the R-shock to supersonic flow in region 5 of Fig. 3b. Guderley's model is commonly known as the four waves theory (4WT), the PM wave being the fourth wave; the 4WT was further modified by Khalghatgi and Hunt [11] by including a slip-stream, shown using a dashed line in Fig. 3b. Kalghatgi and Hunt [11] noticed that in region 4 of Fig. 3b, the flow can be either subsonic or supersonic; in the former case the flow pattern is referred to by [9] as a Vasil'ev reflection (VR), whereas in the latter as a Guderley reflection (GR).

2.2 The (M_1, σ_{12}) plane

A powerful graphical tool for looking at the existence and features of the solutions to both von Neumann's and Guderley's models consists in using a plane where the Mach number, M_1, upstream of the I-shock is on the x-axis and the I-shock local slope, σ_{12}, on the y-axis. The (M_1, σ_{12}) plane is drawn in Fig. 4, where we restrict the abscissas to the M_1-range that is relevant to the applications in Sect. 3 and we only plot the curves which will be referred to throughout the paper. Using the same labeling as in [12], we draw:

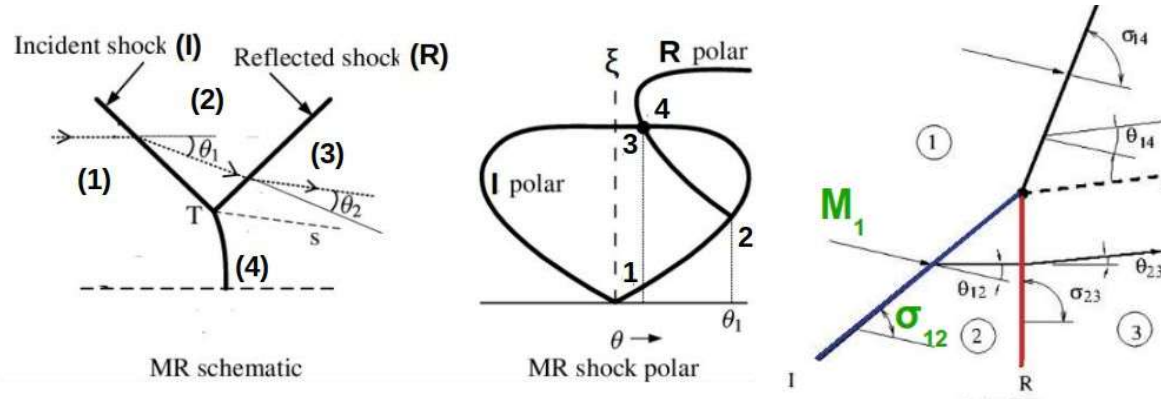

(a) Mach reflection schematic and corresponding shocks poplars (b) 3ST sketch

Figure 2: von Neumann's model (3ST)

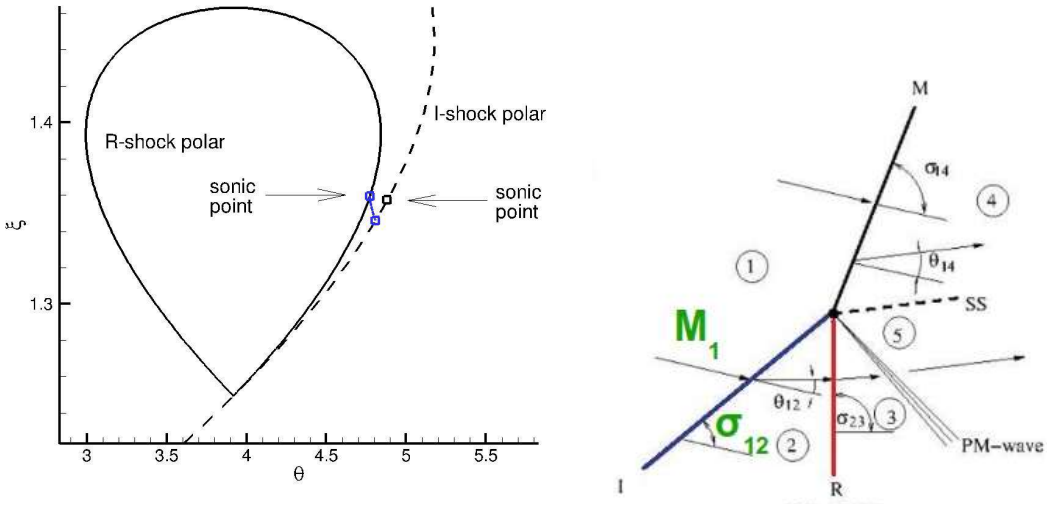

(a) Shock polar (b) 4WT sketch

Figure 3: Guderley's model (4WT)

- Line 1: where the incident shock (I-shock) is a Mach wave;
- Line 2: where the flow is sonic behind I-shock;
- Line 7a: marks the transition between the 3ST and 4WT and is characterized by sonic flow behind the R-shock in the 3ST;
- VR $\Leftrightarrow$ GR: marks the transition between the VR and GR and corresponds to sonic flow behind the M-shock in the 4WT.

The equations required to draw the aforementioned curves can be found in [1]. However, this is only a small subset of the numerous lines that bound regions of the (M_1, σ_{12}) plane where different shock-interaction patterns are observed. The interested reader is referred to [13, 12, 14, 15] for a far more extensive discussion.

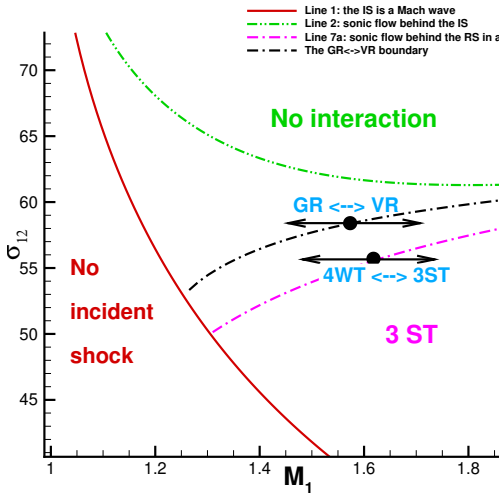

Figure 4: The (M_1, σ_{12}) plane

2.3 CFD solvers

The numerical simulations presented in this study have been carried out using two different CFD solvers. One is the commercial, shock-capturing code `CFD++` [6], which is widely used for simulating flows of aeronautical interest [16, 17] on both structured and unstructured grids. The other is the in-house, shock-fitting code `UnDiFi-2D` which was developed by the authors [7] and is publicly accessible on the GitHub repository `https://github.com/UnDiFi/UnDiFi-2D`. `UnDiFi-2D` is capable of simulating shock/shock and shock/wall interactions in both steady and unsteady flows using 2D unstructured triangular grids; references [18, 19, 20, 21] give examples of inviscid and viscous flow computations performed using `UnDiFi-2D` which highlight the main features of this shock-fitting technique as well as the advantages it offers over state-of-the-art shock-capturing codes when computing high-speed shocked-flows. In all numerical simulations performed using `UnDiFi-2D` in Sect. 4 all shocks and slip-streams are fitted, i.e. treated as true mathematical discontinuities of zero thickness that bound regions of the flow-field where a smooth solution to the governing PDEs exists; see [22, 23, 7] for algorithmic details. In addition, also those branching points where different discontinuities meet are treated as geometrical points (0-dimensional) and modeled as described in [24, 18]. The available interaction models include the 3ST and 4WT, the latter being recently used to model the fishtail shock-pattern around the NACA0012 airfoil [1].

All numerical simulations included in this paper, performed either using `CFD++` or `UnDiFi-2D`, rely on second-order-accurate spatial discretization schemes.

3 Test-case definition

To investigate the properties of the fishtail shock-structure, we simulated the inviscid transonic flow through the channel shown in Fig. 5a. A subsonic flow with constant total pressure and temperature and horizontal velocity is prescribed along the inlet section of the duct, whereas a subsonic flow with

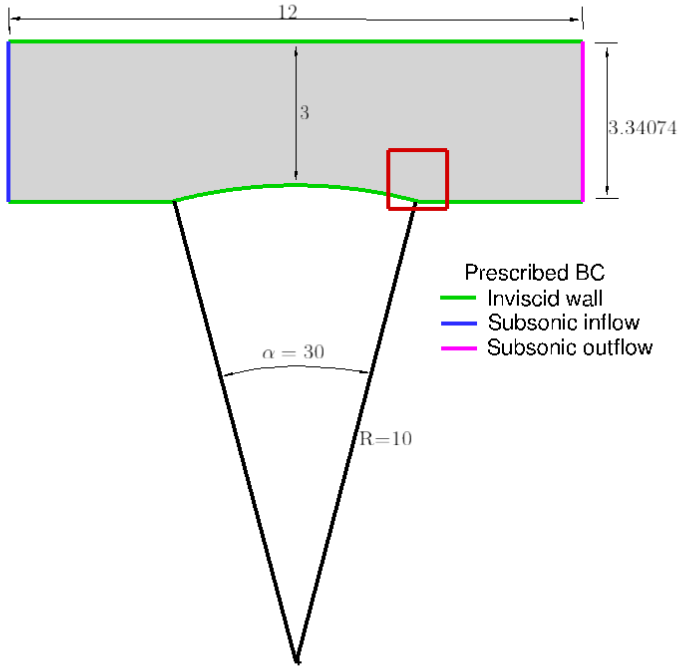

(a) Computational domain and boundary conditions

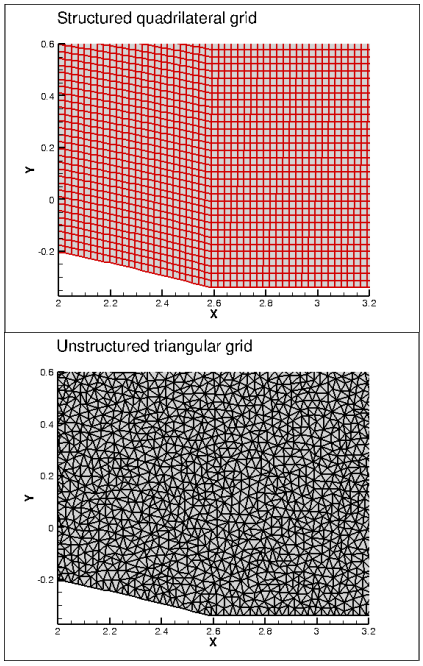

(b) Computational grids.

Figure 5: Computational domain, boundary conditions and grids

Table 1: Boundary conditions defining the various test-cases and features of the grids

(a) Labeling of the test-cases

Test-case label	$\frac{p_e}{p_0}$
D5-1	0.64536
D5-2	0.64355
D5-3	0.64330
D5-4	0.64289
D5-5	0.64247
D5-6	0.64206

(b) Computational grids details

Structured grid		Unstructured grid	
Nodes	Cells	Nodes	Cells
58201	57600	40600	79998

prescribed static pressure is set along the outflow section. The lower wall of the channel has the shape of a circular arc of radius $R = 10$ which subtends an angle equal to $\alpha = 30°$, see Fig. 5a. Two discontinuities in the slope of the lower wall are located where the circular arc joins the straight horizontal wall of the wider sections of the channel. Transonic flow takes place in the duct provided that the pressure ratio (p_e/p_0), defined as the ratio between the static pressure along the exit section and the total pressure along the inlet section, is varied within a suitable range. When operating in the transonic regime, the incoming subsonic flow decelerates and compresses along the lower wall up to the stagnation point located at the leading edge (LE) of the profile, then it expands and accelerates to supersonic conditions along the profile. An oblique shock takes place at the trailing edge (TE) of the profile, because of the slope discontinuity. In these flow conditions a fishtail shock-pattern, similar to the one shown in Fig. 1, may develop. Compared to the *external* flow past the NACA0012 profile which we studied in [1], the chosen *internal* flow test-case offers a significant advantage. Indeed, numerical simulations of transonic external flows require a large computational domain owing to the relatively large size of the supersonic bubbles, see Fig. 1, but also because the distance (X_s in Fig. 1) between the nearly normal shock and the TE is very sensitive to the location of the far-field boundary [25]. The chosen internal flow test-case can instead be computed using a small domain, thus reducing the computational cost.

Table 1a lists the various flow configurations analyzed in this study: each test-case is characterized by a different value of the p_e/p_0 ratio. It is important to note that the p_e/p_0 ratio spans a very small interval. Despite of this, the transonic flow undergoes important and significant topological changes that

will be analyzed in the next sections.

Running test-cases featuring p_e/p_0 values which only differ in the fourth digit poses serious repeatability issues, which become even more severe when different CFD solvers are used. Indeed, unless due care is exercised when running the test-cases listed in Tab. 1a with two different solvers, two very different solutions might be obtained. Differences may be caused by numerical errors, insufficient iterative convergence and differences in the way boundary conditions are prescribed in the two codes, e.g. weak versus strong boundary conditions. For theses reasons, it is necessary to use very fine meshes, accurately verify that the numerical solutions are converged to steady state and that the same p_e/p_0 ratio is indeed prescribed by both CFD solvers.

Two meshes have been used to discretize the computational domain shown in Fig. 5a. The first one is a structured quadrilateral grid and it was used to compute the S-C solution with the `CFD++` code; the second one is an unstructured, triangular mesh, which has been used by `UnDiFi-2D` to compute the S-F solutions. Table 1b reports the number of grid-points and cells for each mesh. Since the meshes are too fine to be displayed, Figs. 5b only shows an enlargement of both in the neighborhood of the TE, i.e. the region bounded by a red box in Fig. 5a. It is worth noting that, even if the structured and unstructured grids are characterized by a different number of grid-points and cells, see Tab. 1b, they share the same number and geometrical location of the grid-points along the domain boundaries.

4 Numerical results

4.1 Shock-capturing results

We here examine the six test-cases listed in Tab. 1a with p_e/p_0 ranging between 0.64536 and 0.64206. Figure 6 collects the pressure contours computed for all six test-cases using `CFD++` on the structured grid. Solutions on the left column were computed starting from the D5-1 case, then decreasing the p_e/p_0 ratio to obtain the solutions of the remaining five test-cases. The sequence of frames on the left of Fig. 6 highlights how tiny variations in the pressure ratio, often of the order of one thousandth, cause remarkable changes in the flow topology. For example, the D5-1 and D5-2 solutions feature a single strong curved shock originating at the TE, whereas all other test-cases exhibit the fishtail shock-pattern. It is also seen that the shock interaction point moves downstream when gradually decreasing the pressure ratio from D5-3 to D5-6.

Frames in the right column of Fig. 6 are the numerical solutions of the same test-cases, but they were computed starting from the D5-6 case (which corresponds to $p_e/p_0 = 0.64206$) and then increasing the p_e/p_0 ratio to obtain the remaining five solutions. All corresponding solutions of the left and right columns of Fig. 6 can be superimposed, except the solutions of the D5-2 test-case. More precisely, the solution on the right column exhibits a fishtail pattern, whereas the solution on the left features a single strong curved shock. To determine which kind of interaction, whether a von Neumann (vNR), Guderley (GR) or Vasil'ev (VR) reflection characterizes each test-case, we extracted from the `CFD++` calculations the (M_1, σ_{12}) pairs close to the branching point and plotted them in the (M_1, σ_{12}) plane. More precisely, the Mach number, M_1, ahead of the I-shock is probed from the CFD solutions, whereas the I-shock local slope, σ_{12}, is obtained from the computed pressure ratio across the I-shock. There clearly is some uncertainty in the extraction process, because in the S-C calculation the branching point is not a geometrical point, but rather a region whose size is of the order of the numerical shock thickness. The D5-1 solution has not been included in the analysis (the same is true for the D5-2 solution shown on the left column of Fig. 6) because no interaction takes place. The D5-2 solution shown on the right column of Fig. 6 was instead included in the analysis.

Figure 7 shows the corresponding points on the (M_1,σ_{12}) plane of the five solutions which exhibit the fishtail pattern. The situation on the M_1,σ_{12} plane is quite complex and reveals unexpected topological differences. From the position of the points observed in Fig. 7, we conclude that the interaction of the D5-2 solution is a GR and, therefore, should be analytically modeled using the 4WT. In the D5-6 solution, however, the interaction is a vNR which should be modeled instead using the 3ST. The interaction of the D5-5 case could also be a vNR, like the D5-6 case. However, we use the conditional because this point is very close to the boundary separating the domain of existence of the 3ST and 4WT and the uncertainty that affects the extraction process does not guarantee the correctness of this finding. The interactions of the D5-3 and D5-4 cases appear to be in region of the VR.

It is worth underlining that this change in the nature of the fishtail interaction point occurs over a very narrow range of pressure ratios. Furthermore, the S-C numerical solutions, even if calculated on fine grids, do not allow to precisely identify the characteristics of the interaction point, i.e. whether it

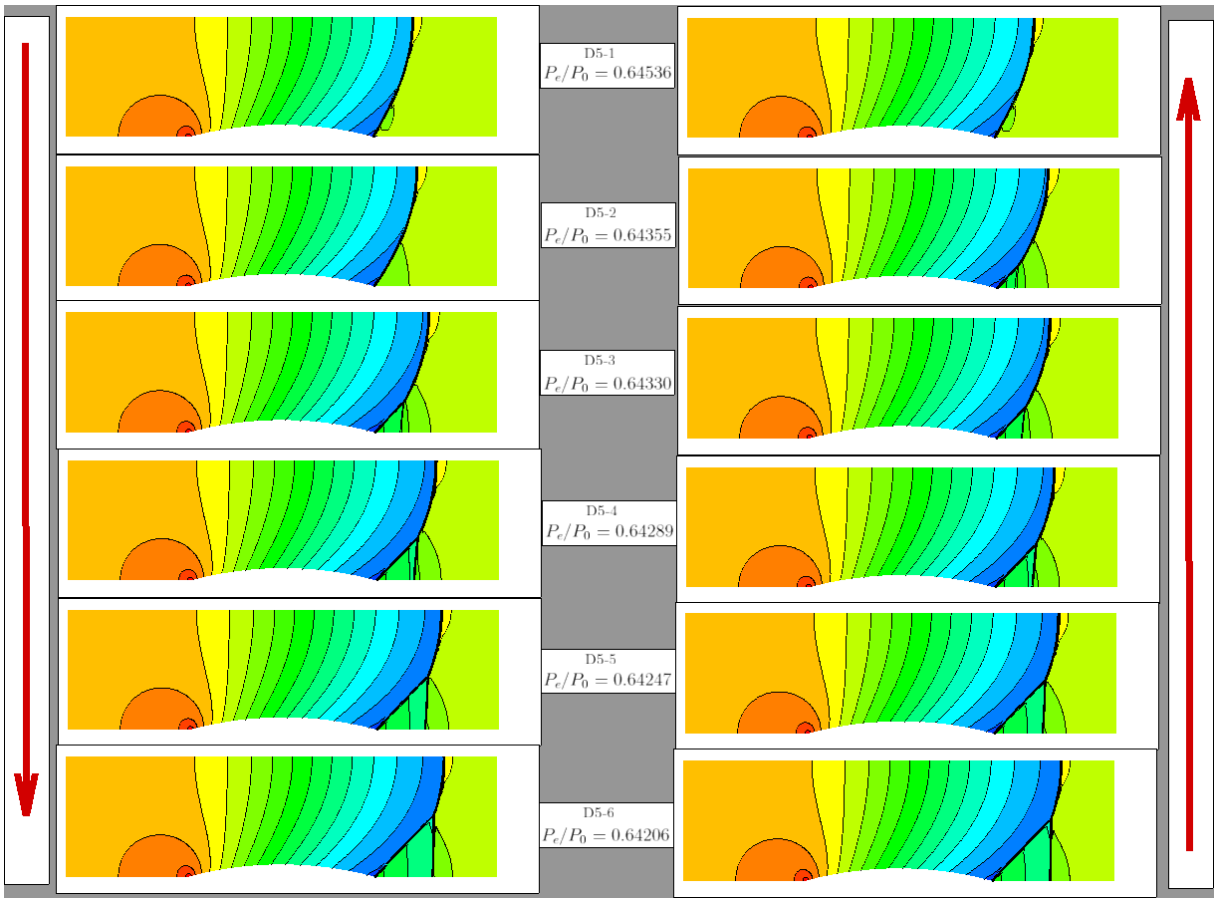

Figure 6: Pressure contour lines of the S-C numerical solutions of the D5-X cases; solution on the left are computed decreasing the p_e/p_0 ratio, solution on the left are computed increasing the p_e/p_0 ratio

is a vNR, GR or VR. This is because the numerical thickness of the shocks and the interaction point does not allow to distinguishing the R-shock from the PM wave, because these waves are tightly packed together, see Fig. 3b, and, furthermore, the PM wave disappears very close to the interaction point. A direct verification of these findings will be possible only by means of S-F simulations where the thickness of the shock waves and the interaction point is reduced to zero and the interaction point is modeled using either the 3ST or the 4WT.

4.2 Shock-fitting results

Results obtained with the S-F approach will be presented in the talk.

5 Conclusions

Transonic flows in a duct with a 30° circular bump on the lower wall have been computed using both the shock-capturing technique implemented in the commercial `CFD++` code and the shock-fitting technique implemented by the authors in the `UnDiFi-2D` open-source code. The analysis of the results showed that: i) within a narrow range of pressure ratios the flow exhibits a shock interaction pattern known as the "fishtail"; ii) within this range of pressure ratios there exists a sub-interval in which two distinct solutions are observed: one characterized by the presence of the fishtail and the other by a strong curved shock; iii) as the pressure ratio p_e/p_0 changes, the interaction point of the fishtail changes nature, taking either the form of a von Neumann, Vasil'ev or Guderley interaction.

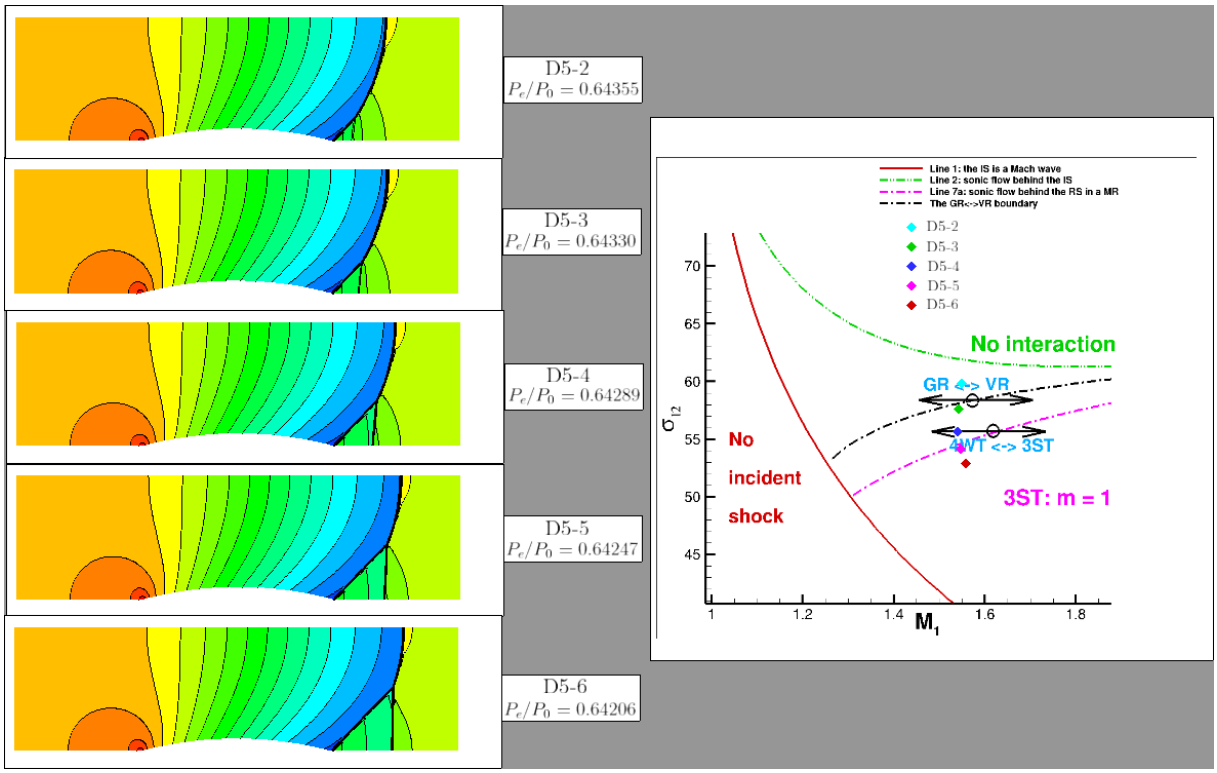

Figure 7: Location of interactions of the D5-X cases in the (M_1, σ_{12}) plane

References

[1] R. Paciorri, A. Bonfiglioli, and A. Assonitis. Features of "fishtail" shock interaction in transonic flows on a naca0012 profile. *AIAA Journal*, 2024.

[2] Renato Paciorri, Aldo Bonfiglioli, and Alessia Assonitis. The transonic flow past a naca0012 and the von neumann paradox. In *AIAA AVIATION 2022 Forum*, page 3990, 2022.

[3] J. Von Neumann. Theory of shock waves. Technical report, Institute for Advanced Study Princeton, NJ, 1943.

[4] J. von Neumann. *The Collected Works of John von Neumann: Volume VI: Theory of Games, Astrophysics, Hydrodynamics and Meteorology*. Pergamon Press, 1963.

[5] K. G. Guderley. Considerations of the structure of mixed subsonic-supersonic flow patterns. Air material command tech. report, F-TR-2168-ND, ATI No. 22780, U.S. Wright-Patterson Air Force Base, GS-AAF-Wright Field 39, Dayton, Ohio., oct 1947.

[6] Sukumar Chakravarthy, Oshin Peroomian, Uriel Goldberg, and Sampath Palaniswamy. The cfd++ computational fluid dynamics software suite. In *AIAA and SAE, 1998 World Aviation Conference*, page 5564, 1998.

[7] L. Campoli, A. Assonitis, M. Ciallella, R. Paciorri, A. Bonfiglioli, and M. Ricchiuto. Undifi-2d: an unstructured discontinuity fitting code for 2d grids. *Computer Physics Communications*, 271:108202, 2022.

[8] R. Courant and K. O. Friedrichs. *Supersonic Flow and Shock Waves*, volume I of *Pure and Applied mathematics*. Interscience Publishers, New York, fourth edition 1963 edition, 1948.

[9] G. Ben-Dor. *Shock wave reflection phenomena*. Springer Verlag, 2007.

[10] K. G. Guderley. *Theory of Transonic Flow*. Pergamon Press, 1962.

[11] G. T. Kalghatgi and B. L. Hunt. The three-shock confluence problem for normally impinging, overexpanded jets. *Aeronautical Quarterly*, 26(2):117–132, 1975.

[12] C. J. Chapman. *High speed flow*. Cambridge University Press, 2000.

[13] H. Hornung. Regular and mach reflection of shock waves. *Annual Review of Fluid Mechanics*, 18(1):33–58, 1986.

[14] C. A. Mouton. *Transition between Regular Reflection and Mach Reflection in the Dual-Solution Domain*. PhD thesis, California Institute of Technology, Pasadena, California, USA, 2007.

[15] V. N. Uskov and M. V. Chernyshov. Special and extreme triple shock-wave configurations. *Journal of Applied Mechanics and Technical Physics*, 47:492–504, 2006.

[16] Uri Goldberg and Yves Allaneau. Contribution from metacomp technologies, inc. to the second high lift prediction workshop. In *52nd Aerospace Sciences Meeting*, page 0912, 2014.

[17] Sukumar Chakravarthy, David Chi, and Uri Goldberg. Flow prediction around the saccon configuration using cfd++. In *28th AIAA Applied Aerodynamics Conference*, page 4563, 2010.

[18] R. Paciorri and A. Bonfiglioli. Shock interaction computations on unstructured, two-dimensional grids using a shock-fitting technique. *Journal of Computational Physics*, 230(8):3155 – 3177, 2011.

[19] A. Bonfiglioli and R. Paciorri. Convergence analysis of shock-capturing and shock-fitting solutions on unstructured grids. *AIAA J.*, 52(7):1404–1416, 2014.

[20] L. Campoli, P. Quemar, A. Bonfiglioli, and M. Ricchiuto. Shock-fitting and predictor-corrector explicit ale residual distribution. In Marcello Onofri and Renato Paciorri, editors, *Shock Fitting: Classical Techniques, Recent Developments, and Memoirs of Gino Moretti*, pages 113–129. Springer International Publishing, Cham, 2017.

[21] A. Assonitis, R. Paciorri, and A. Bonfiglioli. Numerical simulation of shock/boundary-layer interaction using an unstructured shock-fitting technique. *Computers & Fluids*, 228:105058, 2021.

[22] R. Paciorri and A. Bonfiglioli. A shock-fitting technique for 2d unstructured grids. *Computers & Fluids*, 38(3):715–726, 2009.

[23] A. Bonfiglioli, R. Paciorri, and L. Campoli. Unsteady shock-fitting for unstructured grids. *International Journal for Numerical Methods in Fluids*, 81(4):245–261, 2016.

[24] M. S. Ivanov, A. Bonfiglioli, R. Paciorri, and F. Sabetta. Computation of weak steady shock reflections by means of an unstructured shock-fitting solver. *Shock Waves*, 20(4):271–284, 2010.

[25] R. Richter and P. Leyland. Auto-adaptive finite element meshes. In *NASA Langley Research Center, ICASE (LaRC Workshop on Adaptive Grid Methods*, pages 219–232, 1995.